Accurate and systematically improvable density functional theory embedding for correlated wavefunctions

Jason D. Goodpaster, Taylor A. Barnes, Frederick R. Manby, and Thomas F. Miller III

Citation: The Journal of Chemical Physics **140**, 18A507 (2014); doi: 10.1063/1.4864040
View online: http://dx.doi.org/10.1063/1.4864040
View Table of Contents: http://scitation.aip.org/content/aip/journal/jcp/140/18?ver=pdfcov
Published by the AIP Publishing

Accurate and systematically improvable density functional theory embedding for correlated wavefunctions

Jason D. Goodpaster,[1] Taylor A. Barnes,[1] Frederick R. Manby,[2,a)] and Thomas F. Miller III[1,b)]

[1]*Division of Chemistry and Chemical Engineering, California Institute of Technology, Pasadena, California 91125, USA*

[2]*Centre for Computational Chemistry, School of Chemistry, University of Bristol, Bristol BS8 ITS, United Kingdom*

(Received 21 December 2013; accepted 22 January 2014; published online 10 February 2014)

We analyze the sources of error in quantum embedding calculations in which an active subsystem is treated using wavefunction methods, and the remainder using density functional theory. We show that the embedding potential felt by the electrons in the active subsystem makes only a small contribution to the error of the method, whereas the error in the nonadditive exchange-correlation energy dominates. We test an MP2 correction for this term and demonstrate that the corrected embedding scheme accurately reproduces wavefunction calculations for a series of chemical reactions. Our projector-based embedding method uses localized occupied orbitals to partition the system; as with other local correlation methods, abrupt changes in the character of the localized orbitals along a reaction coordinate can lead to discontinuities in the embedded energy, but we show that these discontinuities are small and can be systematically reduced by increasing the size of the active region. Convergence of reaction energies with respect to the size of the active subsystem is shown to be rapid for all cases where the density functional treatment is able to capture the polarization of the environment, even in conjugated systems, and even when the partition cuts across a double bond. © *2014 AIP Publishing LLC*. [http://dx.doi.org/10.1063/1.4864040]

I. INTRODUCTION

The observation that many chemical processes are predominately governed by changes within a localized subsystem has motivated the development of a number of multiscale strategies.[1–24] The success of such methods is contingent on the availability of a sufficiently accurate description of the environment, as well as a suitable model for the coupling between subsystems. Density functional theory (DFT) provides an ideal framework for multiscale embedding.[17–24] In these approaches, an electronic structure calculation on a chemical system is partitioned into calculations on two subsystems: subsystem A, which is treated using an accurate wavefunction theory (WFT), and subsystem B, which is treated using the more computationally efficient DFT method.[25–36] Our projector-based WFT-in-DFT embedding approach has the advantage of offering a framework that is both exact for cases in which both subsystems are treated using DFT (DFT-in-DFT embedding) and efficient for calculations on large systems.[36,37]

Although projector-based embedding is numerically exact for DFT-in-DFT embedding, it is clear that some error is introduced into any practical WFT-in-DFT embedding calculation. Because the energy of the DFT environment is calculated at the DFT level, this contribution will be no more accurate than that of a standard DFT calculation. Evaluation of the interaction between subsystems is also handled using DFT theory, which introduces errors into both the embedding potential of the WFT subsystem, and the nonadditive energy between subsystems. We analyze WFT-in-DFT embedding by decomposing the error into these three contributions, and use the results to suggest further improvements to projector-based embedding. The analysis is performed through careful comparison with local coupled-cluster calculations.

We also analyze the errors of a number of embedding calculations on systems that might be expected to be particularly difficult to treat using projector-based embedding. In particular, we investigate the potential energy surface of a heterolytic bond cleavage using projector-based embedding. As with other local correlation methods, our embedding method exhibits discontinuities in the potential energy surface; however, these discontinuities are small and decrease as the WFT subsystem is expanded. Finally, we consider reactions involving highly conjugated molecules, and find that projector-based embedding produces reliably accurate results for reactions involving moderate changes in polarization.

II. PROJECTOR-BASED EMBEDDING

The projector-based embedding method provides a rigorous framework for embedding a DFT or WFT subsystem description in a DFT environment.[36] In this approach, a Kohn-Sham (KS)-DFT calculation is first performed over the full system. The resulting occupied molecular orbitals (MOs), $\{\phi_i\}$, are then localized and partitioned into the sets $\{\phi_i^{\mathrm{A}}\}$ and

a)Electronic mail: fred.manby@bristol.ac.uk. Present address: California Institute of Technology, Pasadena, California, USA.
b)Electronic mail: tfm@caltech.edu

$\{\phi_i^{\mathrm{B}}\}$, which correspond to subsystems A and B, respectively. These two sets of orbitals are used to form the density matrices of subsystems A and B in the atomic orbital basis, γ^{A} and γ^{B}.

Next, the subsystem Fock matrix is formed for the embedding calculation, such that

$$\mathbf{f}^{\mathrm{A}} = \mathbf{h}^{\mathrm{A\,in\,B}}[\gamma^{\mathrm{A}}, \gamma^{\mathrm{B}}] + \mathbf{g}[\tilde{\gamma}^{\mathrm{A}}], \tag{1}$$

where the embedded core Hamiltonian is

$$\mathbf{h}^{\mathrm{A\,in\,B}}[\gamma^{\mathrm{A}}, \gamma^{\mathrm{B}}] = \mathbf{h} + \mathbf{g}[\gamma^{\mathrm{A}} + \gamma^{\mathrm{B}}] - \mathbf{g}[\gamma^{\mathrm{A}}] + \mu\mathbf{P}^{\mathrm{B}}. \tag{2}$$

Here, $\mathbf{h}$ is the standard one-electron core Hamiltonian, $\mathbf{g}$ includes all the two-electron terms, $\mathbf{P}^{\mathrm{B}}$ is a projection operator, and μ is a level-shift parameter; $\tilde{\gamma}^{\mathrm{A}}$ is the density matrix associated with the MO eigenstates of $\mathbf{f}^{\mathrm{A}}$, $\{\tilde{\phi}_i^{\mathrm{A}}\}$. The projection operator is given by

$$P^{\mathrm{B}}_{\alpha\beta} \equiv \langle b_\alpha | \left\{ \sum_{i\in \mathrm{B}} |\phi_i^{\mathrm{B}}\rangle\langle\phi_i^{\mathrm{B}}| \right\} |b_\beta\rangle, \tag{3}$$

where α, β label the atomic orbital basis functions.[38–45] In the limit of $\mu \to \infty$, the MOs in $\{\tilde{\phi}_i^{\mathrm{A}}\}$ are constrained to be mutually orthogonal with the MOs of subsystem B;[36,37] if in addition the same density functional is used for all calculations, the MOs $\{\tilde{\phi}_i^{\mathrm{A}}\}$ coincide with the original orbitals $\{\phi_i^{\mathrm{A}}\}$.

A self-consistent field optimization, using the Fock matrix $\mathbf{f}^{\mathrm{A}}$, is performed to obtain $\tilde{\gamma}^{\mathrm{A}}$, and the final DFT-in-DFT energy is

$$\begin{aligned} &E_{\mathrm{DFT}}[\tilde{\gamma}^{\mathrm{A}}; \gamma^{\mathrm{A}}, \gamma^{\mathrm{B}}] \\ &\quad = E_{\mathrm{DFT}}[\tilde{\gamma}^{\mathrm{A}}] + E_{\mathrm{DFT}}[\gamma^{\mathrm{B}}] + E^{\mathrm{nad}}_{\mathrm{DFT}}[\gamma^{\mathrm{A}}, \gamma^{\mathrm{B}}] \\ &\qquad + \mathrm{tr}[(\tilde{\gamma}^{\mathrm{A}} - \gamma^{\mathrm{A}})(\mathbf{h}^{\mathrm{A\,in\,B}}[\gamma^{\mathrm{A}}, \gamma^{\mathrm{B}}] - \mathbf{h})], \end{aligned} \tag{4}$$

where E_{DFT} is the standard DFT energy (evaluated with core-Hamiltonian $\mathbf{h}$) and $E^{\mathrm{nad}}_{\mathrm{DFT}}[\gamma^{\mathrm{A}}, \gamma^{\mathrm{B}}]$ is the nonadditive energy between the subsystem densities. The last term is a first-order correction to the difference between $E^{\mathrm{nad}}_{\mathrm{DFT}}[\gamma^{\mathrm{A}}, \gamma^{\mathrm{B}}]$ and $E^{\mathrm{nad}}_{\mathrm{DFT}}[\tilde{\gamma}^{\mathrm{A}}, \gamma^{\mathrm{B}}]$.[31] In the limit of $\mu \to \infty$, $\tilde{\gamma}^{\mathrm{A}} = \gamma^{\mathrm{A}}$ and the DFT-in-DFT embedding energy is identical to the energy from the corresponding KS calculation performed over the full system; as a result, the projector-based approach is numerically exact for DFT-in-DFT embedding calculations.[36] In practice, a large finite value of μ is used, and an additional perturbative correction to the energy can be performed;[36] for appropriate values of μ this correction is typically far smaller than the energy differences discussed in this paper and is thus neglected throughout. Furthermore, as has been previously emphasized, this embedding scheme is exact for any self-consistent field method, such as Hartree-Fock (HF) theory.[36,37]

The nonadditive contribution to the energy, $E^{\mathrm{nad}}_{\mathrm{DFT}}[\gamma^{\mathrm{A}}, \gamma^{\mathrm{B}}]$, can be decomposed into electrostatic and exchange-correlation contributions

$$E^{\mathrm{nad}}_{\mathrm{DFT}}[\gamma^{\mathrm{A}}, \gamma^{\mathrm{B}}] = J^{\mathrm{nad}}[\gamma^{\mathrm{A}}, \gamma^{\mathrm{B}}] + E^{\mathrm{nad}}_{\mathrm{xc}}[\gamma^{\mathrm{A}}, \gamma^{\mathrm{B}}], \tag{5}$$

where

$$J^{\mathrm{nad}}[\gamma^{\mathrm{A}}, \gamma^{\mathrm{B}}] = \int \mathrm{d}r_1 \int \mathrm{d}r_2 \, \frac{\gamma^{\mathrm{A}}(1)\gamma^{\mathrm{B}}(2)}{r_{12}} \tag{6}$$

and

$$E^{\mathrm{nad}}_{\mathrm{xc}}[\gamma^{\mathrm{A}}, \gamma^{\mathrm{B}}] = E_{\mathrm{xc}}[\gamma^{\mathrm{A}} + \gamma^{\mathrm{B}}] - E_{\mathrm{xc}}[\gamma^{\mathrm{A}}] - E_{\mathrm{xc}}[\gamma^{\mathrm{B}}]. \tag{7}$$

The electrostatic term, J^{nad}, is easily evaluated, and although the exact form of E_{xc} is unknown, approximate functionals are well established. Since the embedded MOs $\{\tilde{\phi}_i^{\mathrm{A}}\}$ are orthogonal to those in subsystem B, there is no nonadditivity in the kinetic energy. This removes the requirement of performing optimized effective potential calculations[20,21,23,24,30,31] or using approximate nonadditive kinetic energy functionals.

The projector-based formalism easily allows for WFT-in-DFT embedding, in which subsystem A is treated using a WFT-level description and subsystem B is described at the DFT level.[36] This is achieved by replacing the standard one-electron core Hamiltonian with the embedded core Hamiltonian of Eq. (2). The electronic energy from the WFT-in-DFT embedding approach is

$$\begin{aligned} E_{\mathrm{WFT}}[\Psi^{\mathrm{A}}; \gamma^{\mathrm{A}}, \gamma^{\mathrm{B}}] = &\langle \Psi^{\mathrm{A}} | \hat{H}^{\mathrm{A\,in\,B}}[\gamma^{\mathrm{A}}, \gamma^{\mathrm{B}}] | \Psi^{\mathrm{A}} \rangle \\ &- \mathrm{tr}[\gamma^{\mathrm{A}}(\mathbf{h}^{\mathrm{A\,in\,B}}[\gamma^{\mathrm{A}}, \gamma^{\mathrm{B}}] - \mathbf{h})] \\ &+ E_{\mathrm{DFT}}[\gamma^{\mathrm{B}}] \\ &+ E^{\mathrm{nad}}_{\mathrm{DFT}}[\gamma^{\mathrm{A}}, \gamma^{\mathrm{B}}], \end{aligned} \tag{8}$$

where $|\Psi^{\mathrm{A}}\rangle$ is the embedded wavefunction from the WFT method, and $\hat{H}^{\mathrm{A\,in\,B}}[\gamma^{\mathrm{A}}, \gamma^{\mathrm{B}}]$ is the WFT Hamiltonian resulting from replacing the standard one-electron core Hamiltonian with the embedded core Hamiltonian. The term $\mathrm{tr}[\tilde{\gamma}^{\mathrm{A}}(\mathbf{h}^{\mathrm{A\,in\,B}}[\gamma^{\mathrm{A}}, \gamma^{\mathrm{B}}] - \mathbf{h})]$ is included in the first term of Eq. (8) and thus does not show up in the first-order correction term, as it did in Eq. (4).

III. RESULTS I: SOURCES OF ERROR IN WFT-IN-DFT EMBEDDING

A. Term-by-term comparison with LCSSD(T)

We now formulate an approach to compare the individual terms in the energy expression of a CCSD(T)-in-DFT embedding calculation with the corresponding values calculated at the CCSD(T) level.[46] To do this, we first recognize that the local (L)CCSD(T) method by Schütz and Werner[47–50] becomes exactly equivalent to the canonical CCSD(T) method when all orbital pairs are correlated and all excitation domains are set to the full virtual basis. The terms in the LCCSD(T) energy expression, in turn, can be organized in a way that enables direct comparison to the terms in the CCSD(T)-in-DFT embedding energy expression.

The LCCSD(T) energy can be decomposed as a function of the amplitudes and the atomic-orbital density matrices as

$$\begin{aligned} &E_{\mathrm{LCCSD(T)}}[T_1, T_2, T_3; \gamma^{\mathrm{A}}, \gamma^{\mathrm{B}}] \\ &\quad = + E_{\mathrm{HF}}[\gamma^{\mathrm{A}}] + E^{\mathrm{A}}_{(\mathrm{S})} + E^{\mathrm{A}}_{(\mathrm{D})} + E^{\mathrm{A}}_{(\mathrm{T})} \\ &\qquad + E_{\mathrm{HF}}[\gamma^{\mathrm{B}}] + E^{\mathrm{B}}_{(\mathrm{S})} + E^{\mathrm{B}}_{(\mathrm{D})} + E^{\mathrm{B}}_{(\mathrm{T})} \\ &\qquad + E^{\mathrm{nad}}_{\mathrm{HF}}[\gamma^{\mathrm{A}}, \gamma^{\mathrm{B}}] + E^{\mathrm{nad}}_{(\mathrm{D})} + E^{\mathrm{nad}}_{(\mathrm{T})}, \end{aligned} \tag{9}$$

where E_{HF} is the HF energy and $E_{\mathrm{HF}}^{\mathrm{nad}}[\gamma^{\mathrm{A}}, \gamma^{\mathrm{B}}]$ is the same as Eq. (5), except with the corresponding exchange terms replacing $E_{\mathrm{xc}}^{\mathrm{nad}}[\gamma^{\mathrm{A}}, \gamma^{\mathrm{B}}]$. When the full virtual space is included, the singles are additive and thus there is no nonadditive component. The nonadditive correlation for the double-excitation terms is simply

$$E_{(\mathrm{D})}^{\mathrm{nad}} = E_{(\mathrm{D})} - E_{(\mathrm{D})}^{\mathrm{A}} - E_{(\mathrm{D})}^{\mathrm{B}} \tag{10}$$

and likewise for the triple-excitation correlation energy.

The correlation energy from the single excitations within subsystem A is given by

$$E_{(\mathrm{S})}^{\mathrm{A}} = 2 \sum_{i \in A} \mathbf{f}^{i\dagger} \mathbf{t}^{i}, \tag{11}$$

where the summation spans the occupied orbitals of subsystem A, $\mathbf{f}^i$ is the internal-external part of the Fock matrix in vector form, and $\mathbf{t}^i$ are the single excitation amplitudes in vector form.[47]

The correlation energy from the double excitations within subsystem A is given by

$$E_{(\mathrm{D})}^{\mathrm{A}} = \sum_{\substack{i \geq j \\ i,j \in A}} (2 - \delta_{ij}) \mathrm{tr}[\mathbf{L}^{ij} \mathbf{C}^{ij}], \tag{12}$$

where the summation spans the occupied orbitals of subsystem A, and $\mathbf{L}^{ij}$ are the internal coulomb and exchange matrices. The matrix elements of $\mathbf{C}^{ij}$ are given by $C_{rs}^{ij} = T_{rs}^{ij} + t_r^i t_s^j$, where T_{rs}^{ij} and t_r^i are the double and single excitation amplitudes, respectively.[47]

Finally, the correlation energy from the triple excitations within subsystem A is given by

$$\begin{aligned} E_{(\mathrm{T})}^{\mathrm{A}} = \sum_{\substack{i \geq j \geq k \\ i,j,k \in A}} (2 - \delta_{ij} - \delta_{jk}) \Bigg(& \sum_{rstr'} t_{r'}^i S_{rr'} \, (js|kt) \, X_{rst}^{ijk} \\ & + \sum_{rsts'} t_{s'}^j S_{ss'} \, (ir|kt) \, X_{rst}^{ijk} \\ & + \sum_{rstt'} t_{t'}^k S_{tt'} \, (ir|js) \, X_{rst}^{ijk} + \sum_{rst} W_{rst}^{ijk} X_{rst}^{ijk} \Bigg), \end{aligned} \tag{13}$$

where the first summation spans the occupied orbitals of subsystem A, the indices i, j, k represent occupied orbitals, and the indices r, s, t represent unoccupied orbitals. $S_{rr'}$ is an element of the overlap matrix of the projected atomic orbitals, $(ir|js)$ are two-electron integrals, and t_r^i are the single amplitudes. X_{rst}^{ijk} is defined as $X_{rst}^{ijk} = 4T_{rst}^{ijk} - 2T_{rts}^{ijk} - 2T_{tsr}^{ijk} - 2T_{srt}^{ijk} + T_{trs}^{ijk} + T_{str}^{ijk}$ where T_{rst}^{ijk} are the triples amplitudes. The tensor element W_{rst}^{ijk} contains the double-excitation amplitudes, T_{rs}^{ij}.[48,49]

B. Calculation details

All geometry optimizations are performed using Gaussian09[51] and are provided in the supplementary material.[69] All other calculations are performed in Molpro 2012.1.[52] In all calculations the orbitals are localized using Pipek-Mezey localization.[53] The atoms associated with subsystem A for each reaction are given in the supplementary material.[69] Any localized orbital with a Löwdin charge of 0.4 on an atom associated with subsystem A is included in the set of orbitals associated with subsystem A. All calculations employ a level shift parameter μ, which is set to 10^6 a.u. All KS-DFT calculations employ a large grid for the exchange-correlation functional evaluation, achieved by specifying the Molpro option GRID = 10^{-10}. For computational efficiency, all LCCSD(T) calculations employ density fitting (DF),[54,55] and the triples are approximated using the noniterative (T0) procedure.[48,49] We emphasize that the T0 procedure is only used for calculations involving Eqs. (14), (17), and (18) which arise in our error analysis; this noniterative procedure is not used for any calculations outside of Sec. III C.

To enable the rigorous comparison of terms from the LCCSD(T) calculation and the embedding calculation, some care must be taken. First, all orbital pairs are correlated to recover the energy from canonical CCSD(T). Second, the choice of orbitals must be consistent between the LCCSD(T) and CCSD(T)-in-DFT embedding calculations.

In the WFT-in-DFT embedding method, subsystem B comprises KS MOs, and thus evaluation of the errors resulting from using the DFT energy of subsystem B requires the use of KS MOs as the reference MOs. The difference between canonical CCSD(T) using the HF reference and DF-LCCSD(T0) using the KS reference is within 0.3 mE_{h} for all reactions discussed in Sec. III C, which is smaller than the other sources of error that are analyzed; therefore, throughout Sec. III C, we will simply refer to terms calculated from DF-LCCSD(T0) as CCSD(T).

Likewise, consistent evaluation of the error arising from the embedding potential requires that the reference MOs for the embedded CCSD(T) calculation on subsystem A be obtained from the corresponding DFT calculation. This choice of reference MOs is only used in Sec. III C. In all other sections, the reference MOs of the embedded CCSD(T) calculation are chosen to be the set of MOs resulting from an embedded HF calculation. We note that the difference between CCSD(T)-in-DFT embedding where the MOs for subsystem A are obtained from an embedded DFT calculation compared to an embedded HF calculation is within 0.2 mE_{h} for the reactions considered in Sec. III C.

Below we analyze the contributions to the embedding error for a set of six energies associated with different reactions. All of the chosen reactions are not only large enough to involve partitioning across a covalent bond, but also small enough to allow for calculation of the CCSD(T) reference energy for the full system. The reactions considered are given in Table I.

The data set consists of the following reactions: (1) activation energy for the symmetric S_N2 reaction of Cl^- and propyl chloride; (2) acid hydrolysis of dimethylether to form methanol; (3) deprotonation of the phenol hydroxyl group; (4) ring-closing isomerization of 3-methylene-1-heptene to form butylcylobutane; (5) the Diels-Alder reaction of 2-methoxy-1,3-butadiene with methyl vinyl ketone; and (6) the activation energy for the Diels-Alder reaction. The geometries are provided in the supplementary material.[69]

TABLE I. CCSD(T) reaction energies and barriers in the test set obtained using cc-pVTZ with aug-cc-pV(T+d)Z on Cl, and aug-cc-pVTZ for all atoms for reactions 2–4.[56,57] For ease of error analysis, we adopt a sign convention in which all reactions or activation processes are positive in energy. Geometries were obtained using B3LYP with 6-311G*++ (reaction 1), def2-TZVP (reactions 2–4), or 6-31G* (reactions 5, 6).[58–61]

	Reaction	E/mE_h
1	S_N2 activation barrier	7.8
2	Acid hydrolysis	177.8
3	Phenol deprotonation	568.8
4	Ring closing	10.6
5	Diels-Alder reaction	63.1
6	Diels-Alder barrier	34.0

C. Sources of error in WFT-in-DFT embedding

1. Error from the embedding potential

Now we discuss how comparison of terms in the energy expressions for CCSD(T) and CCSD(T)-in-DFT embedding can be used to determine the error arising from the embedding potential. The energy of subsystem A from the CCSD(T) calculation is the sum of the HF energy (using the KS density) and the correlation energy of subsystem A,

$$E^{\mathrm{A}}_{\mathrm{CCSD(T)}} = E_{\mathrm{HF}}[\gamma^{\mathrm{A}}] + E^{\mathrm{A}}_{(\mathrm{S})} + E^{\mathrm{A}}_{(\mathrm{D})} + E^{\mathrm{A}}_{(\mathrm{T})}. \quad (14)$$

The total energy of subsystem A from a CCSD(T)-in-DFT embedding calculation is

$$E^{\mathrm{A}}_{\mathrm{emb}} = \langle \Psi^{\mathrm{A}} | \hat{H}^{\mathrm{A\,in\,B}}[\gamma^{\mathrm{A}}, \gamma^{\mathrm{B}}] | \Psi^{\mathrm{A}} \rangle - \mathrm{tr}[\gamma^{\mathrm{A}}(\mathbf{h}^{\mathrm{A\,in\,B}}[\gamma^{\mathrm{A}}, \gamma^{\mathrm{B}}] - \mathbf{h})]. \quad (15)$$

For an embedding potential that includes all of the CCSD(T) many-body effects, the energy of $E^{\mathrm{A}}_{\mathrm{CCSD(T)}}$ and $E^{\mathrm{A}}_{\mathrm{emb}}$ would be identical; therefore, the error arising from the embedding potential is calculated as

$$E^{\mathrm{error}}_{\mathrm{pot}} = E^{\mathrm{A}}_{\mathrm{emb}} - E^{\mathrm{A}}_{\mathrm{CCSD(T)}}. \quad (16)$$

The error in the reaction energies arising from the embedding potential is therefore the change in $E^{\mathrm{error}}_{\mathrm{pot}}$ between products and reactants, $\Delta E^{\mathrm{error}}_{\mathrm{pot}}$.

The blue squares in Figure 1 show the value of $\Delta E^{\mathrm{error}}_{\mathrm{pot}}$ for the data set, compared to the total CCSD(T)-in-B3LYP embedding error shown in the black circles. For no system is the error larger than 1.5 mE_h, with the average error being 0.8 mE_h. This demonstrates a key insight of this paper, which is that the embedding potential calculated using WFT-in-DFT embedding is very accurate.

2. Error from use of DFT for subsystem B

Next, we quantify the WFT-in-DFT embedding error resulting from treating subsystem B using DFT. This error is obtained by computing

$$E^{\mathrm{B,error}}_{\mathrm{DFT}} = E_{\mathrm{DFT}}[\gamma^{\mathrm{B}}] - \left(E_{\mathrm{HF}}[\gamma^{\mathrm{B}}] + E^{\mathrm{B}}_{(\mathrm{S})} + E^{\mathrm{B}}_{(\mathrm{D})} + E^{\mathrm{B}}_{(\mathrm{T})}\right), \quad (17)$$

which allows for a direct comparison of the DFT and CCSD(T) energies of subsystem B.

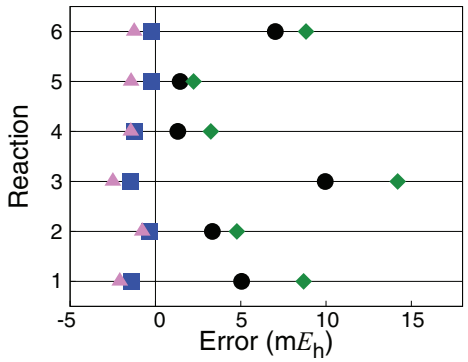

FIG. 1. The error arising from the embedding potential (blue squares), the DFT energy of subsystem B (violet triangles), and the nonadditive exchange-correlation energy (green diamonds) compared to the total CCSD(T)-in-B3LYP embedding error (black circles). CCSD(T) calculations performed on the full system are used as the reference. The largest source of error is the nonadditive exchange-correlation energy functional.

The values calculated for $\Delta E^{\mathrm{B,error}}_{\mathrm{DFT}}$ are shown in Figure 1 as violet triangles. The largest error in this data set is 2.5 mE_h and the average error is 1.5 mE_h. These errors are larger than those resulting from the embedding potential, but are still relatively small compared to the total WFT-in-DFT embedding error. Therefore, for this data set, DFT does an adequate job describing the energy change localized within the environment and is not the dominate source of error.

3. Error from the nonadditive exchange-correlation energy

Finally, we analyze the error that arises from evaluation of the nonadditive exchange-correlation energy with an approximate functional. The error is obtained by computing

$$E^{\mathrm{nad,error}}_{\mathrm{xc}} = E^{\mathrm{nad}}_{\mathrm{DFT}}[\gamma^{\mathrm{A}}, \gamma^{\mathrm{B}}] - \left(E^{\mathrm{nad}}_{\mathrm{HF}}[\gamma^{\mathrm{A}}, \gamma^{\mathrm{B}}] + E^{\mathrm{nad(D)}}_{\mathrm{corr}} + E^{\mathrm{nad(T)}}_{\mathrm{corr}}\right), \quad (18)$$

which allows for the direct comparison of the approximate density functional to the energy obtained at the CCSD(T) level.

The values for $\Delta E^{\mathrm{nad,error}}_{\mathrm{xc}}$ are given in Figure 1 as green diamonds. This term dominates the WFT-in-DFT embedding error, with the largest value of $\Delta E^{\mathrm{nad,error}}_{\mathrm{xc}}$ being 14.2 mE_h, and the average value being 7.2 mE_h. It is thus this term that is responsible for introducing the largest error in the WFT-in-DFT embedding methodology.

The sum of $\Delta E^{\mathrm{error}}_{\mathrm{pot}}$, $\Delta E^{\mathrm{B,error}}_{\mathrm{DFT}}$, and $\Delta E^{\mathrm{nad,error}}_{\mathrm{xc}}$ captures all of the discrepancy between the CCSD(T)-in-DFT calculations and the CCSD(T) calculations performed over the full system. Due to the use of density fitting and the noniterative triples approximation used in the CCSD(T) calculation, the sum of these errors is off by an average of 0.4 mE_h compared to the total CCSD(T)-in-B3LYP embedding error; this makes no difference in the interpretation of the data.

To confirm that our results are not sensitive to the approximate exchange-correlation functional, we repeated the analysis using both PBE[62] and M06[63] (not shown). These conclusions are robust with respect to the approximate

exchange-correlation functional. The nonadditive exchange-correlation energy remains the largest source of error, followed by the DFT energy of subsystem B. Again, we find that DFT, for all of the functionals tested, provides very accurate embedding potentials.

D. Improvement of the nonadditive exchange-correlation energy

Having determined the nonadditive exchange-correlation energy to be the dominate source of error, new algorithms can be proposed to calculate this term more accurately. One approach would be to evaluate the nonadditive exchange exactly and to use a computationally cheap WFT method, such as MP2,[64] to evaluate the nonadditive correlation. The resulting correction to the WFT-in-DFT embedding energy is then

$$E_{\mathrm{xc}}^{\Delta\mathrm{MP2}} = E_{\mathrm{HF}}^{\mathrm{nad}}\left[\tilde{\gamma}_{HF}^{\mathrm{A}}, \gamma^{\mathrm{B}}\right] + \sum_{\substack{i\in A\\ j\in B}}\sum_{rs}\left(2T_{rs}^{ij} - T_{sr}^{ij}\right)K_{rs}^{ij} - E_{\mathrm{DFT}}^{\mathrm{nad}}[\gamma^{\mathrm{A}}, \gamma^{\mathrm{B}}] - \mathrm{tr}\left[\left(\tilde{\gamma}_{\mathrm{HF}}^{\mathrm{A}} - \gamma^{\mathrm{A}}\right)\left(\mathbf{h}^{\mathrm{A\,in\,B}}[\gamma^{\mathrm{A}}, \gamma^{\mathrm{B}}] - \mathbf{h}\right)\right], \quad (19)$$

where $\tilde{\gamma}_{\mathrm{HF}}^{\mathrm{A}}$ is the HF embedded density of subsystem A, T_{rs}^{ij} is the MP2 amplitude, and K_{rs}^{ij} are the exchange two electron integrals.[65] For the MP2 calculation, the orbitals $\{\tilde{\phi}_i^{\mathrm{A}}\} \cup \{\phi_i\}_{\mathrm{B}}$ are used, which allows for the direct calculation of the MP2 correlation between the HF orbitals for A and the KS orbitals of B.

Figure 2 compares the CCSD(T)-in-B3LYP embedding error (black) to the MP2-corrected CCSD(T)-in-B3LYP embedding error (red). The average error of WFT-in-DFT embedding is 4.6 mE_{h}, which drops to 1.2 mE_{h} when the MP2 correction is applied. Alternatively, instead of calculating the full MP2 energy in Eq. (19), one could only calculate the scaled opposite spin (SOS)-MP2 correlation energy.[66] Scaling the opposite spin MP2 correlation by the usual empirical factor of 1.3 leads to the SOS-MP2-corrected CCSD(T)-in-B3LYP embedding error shown in blue in Figure 2. Applying the SOS-MP2 correction results in an average error of 1.1 mE_{h}, which is essentially the same error as that of the full MP2 correction, and only requires computations that scale N^4 compared to N^5 for the full MP2 energy.

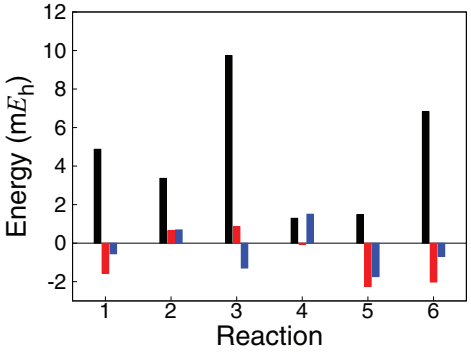

FIG. 2. Bar graph of the error in the energy obtained from CCSD(T)-in-B3LYP embedding (black), MP2-corrected CCSD(T)-in-B3LYP embedding (red), and SOS-MP2-corrected CCSD(T)-in-B3LYP embedding. CCSD(T) calculations performed on the full system are used as the reference.

The average error of standard MP2 calculations on these systems is 6.3 mE_{h} relative to CCSD(T); it is thus clear that effectiveness of the MP2 correction does not rely on the MP2 energy being particularly accurate for the description of the full system. Instead, we observe that MP2 theory accurately represents the correlation energy between subsystems A and B, while not necessarily representing other correlation terms accurately. This is consistent with other local coupled-cluster methods that treat distant pairs at the MP2 level.[47]

IV. RESULTS II: CONTINUITY, CONVERGENCE, AND CONJUGATION IN WFT-IN-DFT EMBEDDING

A. Potential energy surfaces

Next, we examine the potential energy surface for heterolytic bond cleavage. Local correlation methods show discontinuities in the potential energy surface for the heterolytic bond cleavage of CO dissociation in ketene.[67] Here, we study a related system, CO dissociation in 1-penten-1-one.

Figure 3(a) shows potential energy curves calculated using CCSD(T), B3LYP, and CCSD(T)-in-B3LYP embedding. The cc-pVDZ basis was used for all calculations. Here, B3LYP performs relatively well near equilibrium, but overestimates the energy by up to 16 mE_{h} near dissociation. The CCSD(T)-in-B3LYP calculations are very accurate near

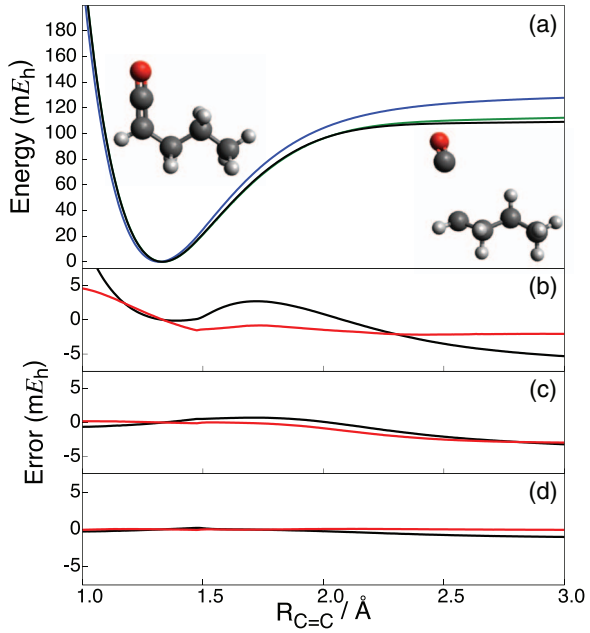

FIG. 3. (a) Potential energy curves for the dissociation of the C-C bond in singlet 1-penten-1-one obtained using CCSD(T) (green), KS-DFT with B3LYP (blue), and CCSD(T)-in-B3LYP embedding (black). The structure was reoptimized at the HF/cc-pVDZ level of theory for each value of the C-C bond distance.[56] The O=C=CH– moiety was treated at the CCSD(T) level for the CCSD(T)-in-B3LYP embedding calculations. (b)–(d) The error in CCSD(T)-in-B3LYP embedding (black) and MP2-corrected CCSD(T)-in-B3LYP embedding (red) as a function of distance between the carbon-carbon double bond. The results are shown for three partitionings of the molecule, with subsystem A corresponding to (b) =C=CH– (18 electrons), (c) O=C=CH– (22 electrons), or (d) O=C=CH–CH_2– (30 electrons).

equilibrium and slightly underestimate the energy near the dissociation limit. MP2-corrected CCSD(T)-in-B3LYP were also performed for this system; the results are not shown in panel A of Figure 3, because they are graphically indistinguishable from the uncorrected CCSD(T)-in-B3LYP results.

Figures 3(b)–3(d) show the error in CCSD(T)-in-B3LYP embedding and MP2-corrected CCSD(T)-in-B3LYP embedding for three different subsystem partitionings of the molecule. The error and the change of the slope at the derivative discontinuity around 1.5 Å decreases by treating more of the system at the CCSD(T) level. Energy discontinuities of 50 μE_h are seen at short distances, as shown in Figure 1 of the supplementary material.[69] Like other local correlation methods, abrupt changes in the localized orbitals for different nuclear configurations lead to discontinuities in the WFT-in-DFT embedding energy and its derivatives. Here, these defects are small and can be systematically controlled by increasing the size of subsystem A.

B. WFT-in-DFT embedding of conjugated systems

A demanding case for any embedding methodology is the partitioning of a π-conjugated system. The applicability of WFT-in-DFT embedding to treat such systems is tested and compared to systems without conjugation.

First, we consider the dissociation of a fluoride anion from both an alkane chain (1-fluorodecane) and an alkene chain (1-fluoro-1,3,5,7,9-decapentaene). The geometries for both compounds and their dissociated products were obtained using B3LYP/def2-TZVP. All CCSD(T) and embedding calculations were performed using the cc-pVDZ basis, with aug-cc-pVDZ for fluorine.[56]

Figure 4(a) shows the CCSD(T)-in-B3LYP with and without the MP2 correction for fluoride anion dissociation from the alkane chain. Results are provided for a number of different choices of the subsystem partitioning, and the error of both methods can be seen to rapidly vanish as more atoms are included in the WFT subsystem.

The individual sources of error in the CCSD(T)-in-B3LYP embedding calculations, computed in the same way as in Sec. III C, are shown in Figure 4(b). Again, it is observed that the error arising from the embedding potential is small, accounting for only a small portion of the total error. Unlike previous results, the error arising from treating subsystem B at the DFT level is of similar magnitude as the nonadditive exchange-correlation energy error. As these errors are of opposite sign, evaluating the nonadditive exchange-correlation energy using DFT leads to a favorable cancelation of error. The MP2 correction only increases the accuracy of the subsystem interaction energy, and cannot be expected to correct large errors associated with the DFT energy of subsystem B.

Figure 4(c) shows the Mulliken population of the density associated with subsystem B on the atoms associated with subsystem A. In the dissociated product, the density associated with subsystem B distributes onto the atoms of subsystem A to stabilize the positive charge. We find that when the difference of this quantity is large between two configurations, there is typically a favorable cancelation of error between the error arising from treating subsystem B using DFT and the error arising from evaluating the nonadditive exchange-correlation energy using DFT. In general, we note that if the nonadditive exchange-correlation is not the dominant source of error, the MP2 correction cannot significantly improve the accuracy of the embedding calculation.

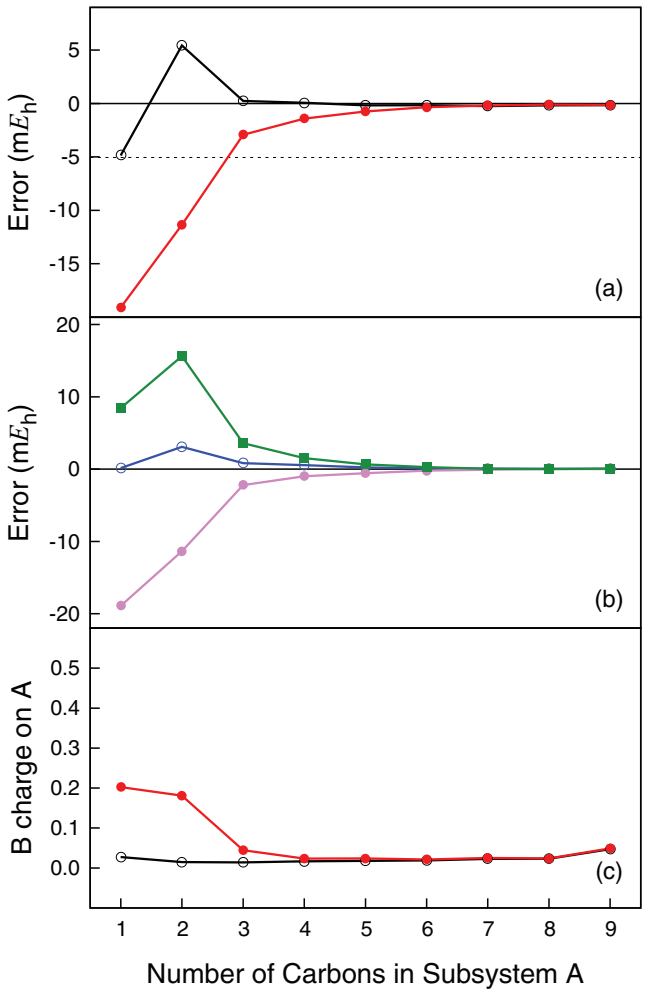

FIG. 4. (a) The error in CCSD(T)-in-B3LYP embedding (black open circles) and MP2-corrected CCSD(T)-in-B3LYP embedding (red filled circles) as a function of the number of carbons included in subsystem A for the dissociation of the alkane. The B3LYP energy is given by the black dotted line. (b) Contributions to the WFT-in-DFT error: embedding potential (blue open circles), DFT for subsystem B (violet filled circles), and DFT for nonadditive exchange-correlation energy (green squares). (c) DFT Mulliken population of the density associated with subsystem B on the atoms in subsystem A, shown for 1-fluorodecane (black open circles) and the dissociated alkane chain (red filled circles).

After dissociation of the fluoride anion from 1-fluoro-1,3,5,7,9-decapentaene, the subsequent geometry optimization leads to an isomerization where the proton on the second carbon moves to the first. Therefore, the analysis for this reaction begins at the second carbon. Figure 5(a) shows the error in CCSD(T)-in-B3LYP embedding (black open circles) and MP2-corrected CCSD(T)-in-B3LYP embedding (red filled circles) as a function of the number of carbons included in subsystem A for fluoride anion dissociation from 1-fluoro-1,3,5,7,9-decapentaene. Unlike the alkane case, the

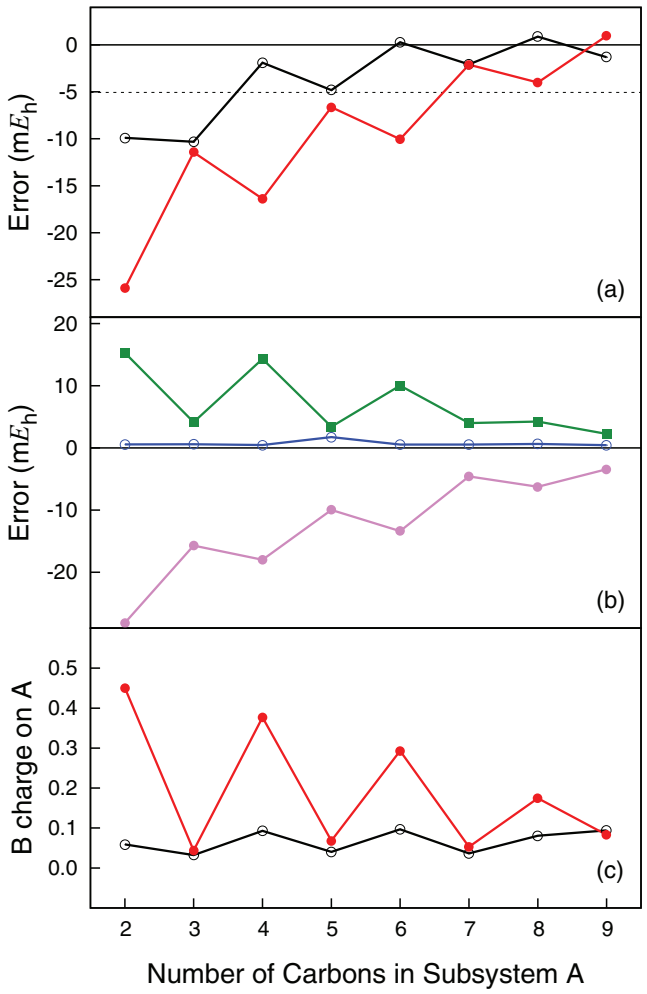

FIG. 5. (a) The error in CCSD(T)-in-B3LYP embedding (black open circles) and MP2-corrected CCSD(T)-in-B3LYP embedding (red filled circles) as a function of the number of carbons included in subsystem A for the dissociation of the alkene. The B3LYP energy is given by the black dotted line. (b) Contributions to the WFT-in-DFT error: embedding potential (blue open circles), use of DFT for subsystem B (violet filled circles), nonadditive exchange-correlation energy (green squares). (c) DFT Mulliken population of the density associated with subsystem B on the atoms in subsystem A, shown for 1-fluoro-1,3,5,7,9-decapentaene (black open circles) and the dissociated alkene chain (red filled circles).

alkene case exhibits large errors which slowly decrease once the majority of the system is treated at the CCSD(T) level.

Figure 5(b) shows the decomposition of the contributions to the error in CCSD(T)-in-B3LYP embedding. In this calculation, the error arising from treating subsystem B using DFT is the dominate source of error. This explains why the error remains large until the majority of the system is treated at the CCSD(T) level, and why the MP2-correction is insufficient to reduce the error.

Figure 5(c) shows the Mulliken population of the density associated with subsystem B on the atoms associated with subsystem A for the alkene case. As with the alkane case, a large difference in this quantity is seen between the fluorinated and defluorinated compounds. This observation provides insight into why the error from the DFT energy of B contributes strongly to the error of the embedding calculations.

TABLE II. The magnitude of the change in the dipole moment between products and reactants for the dissociation of F^- from the alkane and alkene chains, as well as the corresponding magnitudes for the H-F exchange reaction. Values are reported in atomic units.

	Method	Dissociation	Exchange
Alkane	B3LYP	7.338	0.781
	CCSD	7.539	0.802
Alkene	B3LYP	1.702	0.551
	CCSD	3.034	0.630

The magnitude of the change in the dipole moment between the fluorinated and defluorinated compounds is shown in Table II for KS-DFT with B3LYP and CCSD. In the alkane dissociation, the change in the dipole moment is large, demonstrating a small polarizability, and there is good agreement between KS-DFT and CCSD. In the alkene dissociation, the change in dipole moment is considerably smaller than the alkane case, demonstrating that the density polarizes to stabilize charge. For the alkene, there is large disagreement between KS-DFT and CCSD, demonstrating the known failure of DFT to accurately treat polarizability though a π-conjugated system.[68] Therefore, when there are large errors associated with KS-DFT, these large errors will affect the DFT energy of subsystem B, causing large WFT-in-DFT embedding errors. We emphasize that for cases in which DFT does correctly describe the polarization of the environment, this large source of error does not arise. The failure of WFT-in-DFT embedding in Figure 5 is not a failure of embedding itself, but rather a failure of DFT to accurately treat the polarizability of π-conjugated systems.

Finally, we consider the reaction of exchanging the fluoride anion from 1-fluorodecane and 1-fluoro-1,3,5,7,9-decapentaene with a hydride (Figure 6). The change in dipole moment for these reactions is provided in Table II. These reactions exhibit a moderate change in dipole moment, and there is good agreement between CCSD and KS-DFT.

Figures 6(a) and 6(b) plot the error in the CCSD(T)-in-B3LYP embedding and MP2-corrected CCSD(T)-in-B3LYP embedding energies for the hydride exchange reactions from alkane and alkene chains, respectively, as a function of the number of carbons included in subsystem A. For every partition, the errors are small. For the smallest division, the MP2 correction provides a significant improvement in the accuracy of the CCSD(T)-in-B3LYP embedding energy; for larger divisions, the effect of the MP2 correction is much smaller. Unlike in the case of fluoride anion dissociation, DFT applied to the hydride exchange reaction accurately represents the change in dipole. As there are no large errors arising from the DFT energy of subsystem B, WFT-in-DFT embedding performs accurately and the MP2 correction further improves the energetics.

The important observation from these calculations is that when there is a large error in the DFT calculation on the environment, there will be correspondingly large errors in the WFT-in-DFT embedding energy. Importantly, this failure is associated with errors intrinsic to the DFT functionals, and does not arise due to errors in the embedding

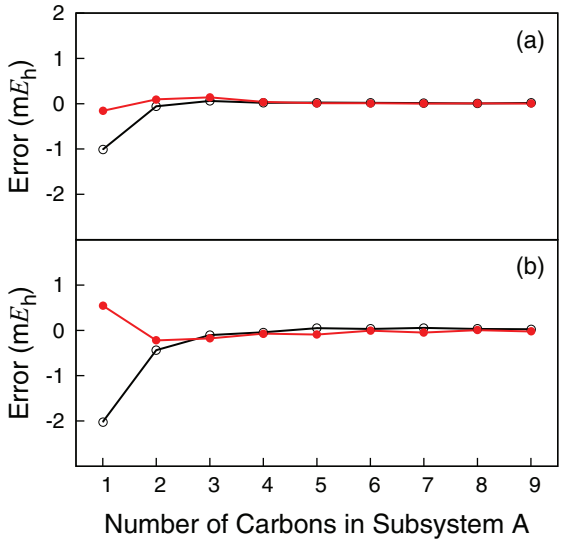

FIG. 6. The error in CCSD(T)-in-B3LYP embedding (black open circles) and MP2-corrected CCSD(T)-in-B3LYP embedding (red filled circles) as a function of the number of carbons included in subsystem A for the exchange of fluoride to a hydride in (a) 1-fluorodecane and (b) 1-fluoro-1,3,5,7,9-decapentaene.

potential. When a chemical process involves a large change in the Mulliken population of subsystem B located on the subsystem A atoms, it is likely that the embedding error will be dominated by errors arising from the DFT-level treatment of subsystem B; errors of this sort cannot be reduced by the MP2 correction.

V. CONCLUSIONS

Projector-based quantum embedding provides a scheme for multiscale descriptions with the exactness property that DFT-in-DFT is equivalent to DFT on the whole system.[36,37] In many tests and applications, we find the accuracy of the scheme to be excellent, allowing for aggressive partitioning across covalent bonds close to the reactive center of the system of interest. However, for some applications, the errors introduced by embedding are larger than would typically be acceptable, and the principal aims of this paper have been to understand and take steps towards resolving the errors in such cases.

Careful comparison of CCSD(T)-in-DFT embedding calculations with CCSD(T) calculations performed over the full system has led to key insights regarding the sources of error in the embedding calculations. First, the embedding potential obtained using approximate density functionals is found to be accurate for all of the cases we have investigated, making a contribution to the overall error of the embedding calculation that is negligible compared to other sources of error. It was not immediately obvious that this would be the case, because functionals (particularly in cases where they are parameterized) are designed with accurate energies in mind.

And second, it is found that in many cases, the primary source of error in CCSD(T)-in-DFT embedding is the treatment of nonadditive exchange-correlation effects with an approximate density functional. This is important because it is the one term in the error for which simple corrections can be developed that conserve the efficiency of the original method. Here, we found that use of MP2 or SOS-MP2 corrections for this term typically improved the accuracy of the energetics for chemical reactions, reducing the average error from 4.6 mE_h to 1.2 mE_h with respect to CCSD(T) calculations performed over the full system.

To investigate the convergence with respect to the size of subsystem A, we studied dissociation and exchange events at the terminus of 10-carbon alkyl and conjugated chains. For the removal of F^-, the results of the CCSD(T)-in-DFT embedding calculation for the conjugated system are noticeably worse than for the alkane, and it is found that the MP2 correction does not reduce this error in the computed reaction energy. Our analysis shows, however, that these results follow from the fact that DFT provides a poor description of the polarization of the charged alkene fragment and that the uncorrected CCSD(T)-in-DFT results benefit from a cancellation of errors in the DFT treatment of subsystem B and in the DFT treatment of nonadditive exchange-correlation. The MP2 correction improves the description of nonadditive energy term, but it does not compensate for the inaccuracies in the DFT description of subsystem B.

For a hydride exchange reaction at the terminus of the alkyl and conjugated chains, the CCSD(T)-in-DFT embedding results converge smoothly and rapidly to reference CCSD(T) calculations performed over the full system, regardless of inclusion of the MP2 correction and regardless of conjugation in the chain. These results demonstrate that in the regime where DFT is adequate for the treatment of the environment, our projector-based embedding scheme can effectively partition the system, even in conjugated molecules.

The current work demonstrates that projection-based embedding provides both a rigorous and practical approach to embedding correlated wavefunctions in a DFT description of the environment. Although the results presented here utilize coupled-cluster methods for describing the correlated wavefuction, we emphasize that projection-based embedding can be combined just as easily with multi-reference electronic structure methods, as well as any mean-field description of the environment. The embedding method is straightforward to employ—requiring only the specification of which atoms are to be treated at the WFT and DFT levels of theory—and it is fully implemented and available in the MOLPRO quantum chemistry package.

ACKNOWLEDGMENTS

This work is supported by the U. S. Army Research Laboratory and the U. S. Army Research Office (USARO) under Grant No. W911NF-10-1-0202 (J.D.G.), by the Air Force Office of Scientific Research (USAFOSR) under Grant No. FA9550-11-1-0288 (T.A.B.), and by the (U.S.) Department of Energy (DOE) under Grant No. DE-SC0006598 (J.D.G.). T.F.M. acknowledges support from a Camille and Henry Dreyfus Foundation Teacher-Scholar Award and an Alfred P. Sloan Foundation Research Fellowship. F.R.M. was visiting Caltech while most of the research was performed. He gratefully acknowledges support for the sabbatical through

a University Research Fellowship from the Institute of Advanced Studies at the University of Bristol and a Royal Society Wolfson Research Merit Award.

[1]A. Warshel and M. Karplus, J. Am. Chem. Soc. **94**, 5612 (1972).
[2]A. Warshel and M. Levitt, J. Mol. Biol. **103**, 227 (1976).
[3]P. Sherwood, A. H. de Vries, S. J. Collins, S. P. Greatbanks, N. A. Burton, M. A. Vincent, and I. H. Hillier, Faraday Discuss. **106**, 79 (1997).
[4]J. L. Gao, P. Amara, C. Alhambra, and M. J. Field, J. Phys. Chem. A **102**, 4714 (1998).
[5]H. Lin and D. G. Truhlar, Theor. Chem. Acc. **117**, 185 (2007).
[6]H. M. Senn and W. Thiel, Angew. Chem., Int. Ed. **48**, 1198 (2009).
[7]L. Hu, P. Söderhjelm, and U. Ryde, J. Chem. Theory Comput. **7**, 761 (2011).
[8]S. Dapprich, I. Komáromi, K. S. Byun, K. Morokuma, and M. J. Frisch, J. Mol. Struct.: THEOCHEM **461–462**, 1 (1999).
[9]F. Maseras and K. Morokuma, J. Comput. Chem. **16**, 1170 (1995).
[10]K. Kitaura, E. Ikeo, T. Asada, T. Nakano, and M. Uebayasi, Chem. Phys. Lett. **313**, 701 (1999).
[11]D. G. Federov and K. Kitaura, J. Chem. Phys. **120**, 6832 (2004).
[12]D. G. Federov and K. Kitaura, J. Phys. Chem. A **111**, 6904 (2007).
[13]P. Arora, W. Li, P. Piecuch, J. W. Evans, M. Albao, and M. S. Gordon, J. Phys. Chem. C **114**, 12649 (2010).
[14]S. R. Pruitt, M. A. Addicoat, M. A. Collins, and M. S. Gordon, Phys. Chem. Chem. Phys. **14**, 7752 (2012).
[15]K. R. Brorsen, N. Minezawa, F. Xu, T. L. Windus, and M. S. Gordon, J. Chem. Theory Comput. **8**, 5008 (2012).
[16]A. Gaenko, T. L. Windus, M. Sosonkina, and M. S. Gordon, J. Chem. Theory Comput. **9**, 222 (2013).
[17]G. Senatore and K. Subbaswamy, Phys. Rev. B **34**, 5754 (1986).
[18]P. Cortona, Phys. Rev. B **44**, 8454 (1991).
[19]T. A. Wesolowski and A. Warshel, J. Phys. Chem. **97**, 8050 (1993).
[20]J. D. Goodpaster, N. Ananth, F. R. Manby, and T. F. Miller III, J. Chem. Phys. **133**, 084103 (2010).
[21]J. D. Goodpaster, T. A. Barnes, and T. F. Miller III, J. Chem. Phys. **134**, 164108 (2011).
[22]Ł. Rajchel, P. S. Żuchowski, M. M. Szczęśniak, and G. Chałasiński, Chem. Phys. Lett. **486**, 160 (2010).
[23]S. Fux, C. R. Jacob, J. Neugebauer, L. Visscher, and M. Reiher, J. Chem. Phys. **132**, 164101 (2010).
[24]J. Nafziger, Q. Wu, and A. Wasserman, J. Chem. Phys. **135**, 234101 (2011).
[25]N. Govind, Y. A. Yang, A. J. R. da Silva, and E. A. Carter, Chem. Phys. Lett. **295**, 129 (1998).
[26]N. Govind, Y. A. Wang, and E. A. Carter, J. Chem. Phys. **110**, 7677 (1999).
[27]A. S. P. Gomes, C. R. Jacob, and L. Visscher, Phys. Chem. Chem. Phys. **10**, 5353 (2008).
[28]T. A. Wesolowski, Phys. Rev. A **77**, 012504 (2008).
[29]Y. G. Khait and M. R. Hoffmann, J. Chem. Phys. **133**, 044107 (2010).
[30]C. Huang, M. Pavone, and E. A. Carter, J. Chem. Phys. **134**, 154110 (2011).
[31]C. Huang and E. A. Carter, J. Chem. Phys. **135**, 194104 (2011).
[32]S. Hofener, A. S. P. Gomes, and L. Visscher, J. Chem. Phys. **136**, 044104 (2012).
[33]O. Roncero, A. Zanchet, P. Villarreal, and A. Aguado, J. Chem. Phys. **131**, 234110 (2009).
[34]A. Severo Pereira Gomes and C. R. Jacob, Annu. Rep. Prog. Chem., Sect. C: Phys. Chem. **108**, 222 (2012).
[35]J. D. Goodpaster, T. A. Barnes, F. R. Manby, and T. F. Miller III, J. Chem. Phys. **137**, 224113 (2012).
[36]F. R. Manby, M. Stella, J. D. Goodpaster, and T. F. Miller III, J. Chem. Theory Comput. **8**, 2564 (2012).
[37]T. A. Barnes, J. D. Goodpaster, F. R. Manby, and T. F. Miller III, J. Chem. Phys. **139**, 024103 (2013).
[38]P. G. Lykos and R. G. Parr, J. Chem. Phys. **24**, 1166 (1956).
[39]J. C. Phillips and L. Kleinman, Phys. Rev. **116**, 287 (1959).
[40]A. A. Cantu and S. Huzinaga, J. Chem. Phys. **55**, 5543 (1971).
[41]H. Stoll, B. Paulus, and P. Fulde, J. Chem. Phys. **123**, 144108 (2005).
[42]R. A. Mata, H.-J. Werner, and M. Schütz, J. Chem. Phys. **128**, 144106 (2008).
[43]T. M. Henderson, J. Chem. Phys. **125**, 014105 (2006).
[44]B. Swerts, L. F. Chibotaru, R. Lindh, L. Seijo, Z. Barandiaran, S. Clima, K. Pierloot, and M. F. A. Hendrickx, J. Chem. Theory Comput. **4**, 586 (2008).
[45]J. L. Pascual, N. Barros, Z. Barandiaran, and L. Seijo, J. Phys. Chem. A **113**, 12454 (2009).
[46]C. Hampel, K. Peterson, and H.-J. Werner, Chem. Phys. Lett. **190**, 1 (1992).
[47]C. Hampel and H.-J. Werner, J. Chem. Phys. **104**, 6286 (1996).
[48]M. Schütz and H.-J. Werner, Chem. Phys. Lett. **318**, 370 (2000).
[49]M. Schütz, J. Chem. Phys. **113**, 9986 (2000).
[50]M. Schütz, G. Rauhut, and H.-J. Werner, J. Phys. Chem. A **102**, 5997 (1998).
[51]M. J. Frisch, G. W. Trucks, H. B. Schlegel *et al.*, Gaussian 09, Gaussian, Inc., Wallingford, CT, 2009.
[52]H.-J Werner, P. J. Knowles, R. Lindh, F. R. Manby, M. Shütz *et al.*, MOLPRO, version 2012.1, a package of *ab initio* programs, 2012, see www.molpro.net.
[53]J. Pipek and P. Mezey, J. Chem. Phys. **90**, 4916 (1989).
[54]M. Schütz and F.-R. Manby, Phys. Chem. Chem. Phys. **5**, 3349 (2003).
[55]H.-J. Werner and M. Schütz, J. Chem. Phys. **135**, 144116 (2011).
[56]T. H. Dunning, Jr., J. Chem. Phys. **90**, 1007 (1989).
[57]T. H. Dunning, Jr., K. A. Peterson, and A. K. Wilson, J. Chem. Phys. **114**, 9244 (2001).
[58]A. D. Becke, J. Chem. Phys. **98**, 5648 (1993).
[59]J. A. Pople and P. C. Haharan, Theor. Chim. Acta **28**, 213 (1973).
[60]F. Weigend and R. Ahlrichs, Phys. Chem. Chem. Phys. **7**, 3297 (2005).
[61]W. J. Hehre, R. Ditchfield, and J. A. Pople, J. Chem. Phys. **56**, 2257 (1972).
[62]J. P. Perdew, K. Burke, and M. Ernzerhof, Phys. Rev. Lett. **77**, 3865 (1996).
[63]Y. Zhao and D. G. Truhlar, Theor. Chem. Acc. **120**, 215 (2008).
[64]C. Møller and M. S. Plesset, Phys. Rev. **46**, 0618 (1934).
[65]M. Schütz, G. Hetzer, and H.-J. Werner, J. Chem. Phys. **111**, 5691 (1999).
[66]Y. Jung, R. C. Lochan, A. D. Dutoi, and M. Head-Gordon, J. Phys. Chem. **121**, 9793 (2004).
[67]N. J. Russ and T. D. Crawford, J. Chem. Phys. **121**, 691 (2004).
[68]H. L. Woodcock, H. F. Schaefer III, and P.-R. Schreiner, J. Phys. Chem. A **106**, 11923 (2002).
[69]See supplementary material at http://dx.doi.org/10.1063/1.4864040 for molecular geometries and additional results.